Published in final edited form as:

Neuroscience. 2019 February 10; 399: 53–64. doi:10.1016/j.neuroscience.2018.12.025.

ADAMTS18 Deficiency Affects Neuronal Morphogenesis and Reduces the Levels of Depression-like Behaviors in Mice

Rui Zhu[a], **Yi-Hsuan Pan**[a], **Lijie Sun**[a], **Tianhao Zhang**[a], **Caiyun Wang**[a], **Shuai Ye**[a], **Ning Yang**[a], **Tiantian Lu**[a], **Thomas Wisniewski**[b], **Suying Dang**[c,*], **Wei Zhang**[a,*]

[a]Key Laboratory of Brain Functional Genomics, Ministry of Education, Shanghai Key Laboratory of Brain Functional Genomics, School of Life Science, East China Normal University, China

[b]Departments of Neurology, Pathology and Psychiatry, New York University School of Medicine, New York, NY 10016, USA

[c]Department of Biochemistry and Molecular Cell Biology, Shanghai Jiao Tong University School of Medicine, Shanghai, China

Abstract

The ADAMTS (a disintegrin and metalloproteinase with thrombospondin motifs) enzymes are secreted, multi-domain matrix-associated zinc metalloendopeptidases that modify extracellular matrix components and play crucial roles in development and numerous diseases. ADAMTS18 is a member of the ADAMTS family, and genome-wide association studies made an initial association of ADAMTS18 with white matter integrity in healthy people of 72–74 years old. However, the potential roles of ADAMTS18 in central nervous system remain unclear. In this study, we showed that *Adamts18* mRNA is highly abundant in developing brains, especially in the cerebellum granular cell layer and the hippocampus dentate gyrus (DG) granular cell layer. *Adamts18* knockout (KO) mice displayed higher dendritic branching complexity and spine density on hippocampal DG granular cells. Behavioral tests showed that *Adamts18* KO mice had reduced levels of depression-like behaviors compared to their wild-type (WT) littermates. The increased neurite formation could be attributed in part to reduced phosphorylation levels of the collapsin response mediator protein-2 (CRMP2) due to activation of the laminin/PI3K/AKT/GSK-3β signaling pathway. Our findings revealed a critical role of ADAMTS18 in neuronal morphogenesis and emotional control in mice.

Keywords

ADAMTS18; laminin; dendritic branching; depression

*Corresponding authors. Address: East China Normal University, 3663 North Zhongshan Road, Shanghai 200062, China (W. Zhang). suyingdang@shsmu.edu.cn (S. Dang), wzhang@sat.ecnu.edu.cn (W. Zhang).

CONFLICT OF INTEREST

The authors declare no competing interests.

INTRODUCTION

The ADAMTS (a disintegrin and metalloproteinase with thrombospondin motifs) family includes 19 secreted metalloproteinases that modify extracellular components and play important roles in the regulation of multiple physiological processes and pathological conditions, such as tissue morphogenesis, fertility, inflammation, tumorigenesis, and vascular functions (Porter et al., 2005; Apte, 2009; Wei et al., 2014; Kelwick et al., 2015). ADAMTSs are highly expressed in the spinal cord, brain stem, hippocampus, striatum, and cortex (Gottschall and Howell, 2015). Most ADAMTSs are produced by astrocytes, neurons, and microglia (Lemarchant et al., 2013). The functions of ADAMTSs in the central nervous system (CNS) remain unclear. However, it has been shown that ADAMTSs (ADAMTS-1, −4, −5, −9) play a role in recovery and repair following spinal cord injury and seizure-induced neural damage by stimulating axonal outgrowth, and enhancing synaptic plasticity in the brain (Lemarchant et al., 2013; Gottschall and Howell, 2015).

ADAMTS18, an orphan ADAMTS, remains to be characterized with regard to its functions and substrates. In humans, *ADAMTS18* mutations have been linked to tumorigenesis (Jin et al., 2007), developmental eye disorders (Aldahmesh et al., 2011, 2013; Peluso et al., 2013), and reduced bone mineral density (BMD) (Xiong et al., 2009). ADAMTS18 is most highly expressed in the brain (Apte, 2009; Wei et al., 2014). A genome-wide association study (GWAS) of 542,050 single-nucleotide polymorphisms (SNPs) in healthy people of 72–74 years old showed that ADAMTS18 is associated with white matter integrity in the brain (Lopez et al., 2012). Among the SNPs, rs7192208, located in an intron of the *ADAMTS18* gene, has the strongest association. However, the roles of ADAMTS18 on CNS development and functions remain unclear.

ADAMTS18 is relatively well conserved in evolution. Murine ADAMTS18 is 89% homologous with human ADAMTS18 (https://blast.ncbi.nlm.nih.gov/). To elucidate its function, we generated an *Adamts18* KO mouse strain (Lu et al., 2017). In this study, we use this mouse model to determine the functions of ADAMTS18 in brain development. We demonstrated for the first time that ADAMTS18 plays a crucial role in neuronal morphogenesis and emotional control in mice.

EXPERIMENTAL PROCEDURES

Reagents

All reagents were purchased from Sigma–Aldrich (St. Louis, MO, USA) unless otherwise indicated. Primary antibodies used in this study are listed in Table 1.

Animals

Adamts18 KO and wild-type (WT) mice with the C57BL/6/129Sv background were generated and genotyped as previously described (Lu et al., 2017). Male mice at 8–10 weeks of age were used for all behavioral tests. Animals were maintained on a 12-h light/dark schedule (lights on at 06:00) in a specific pathogen-free facility. Mice for behavioral tests were housed in groups of 5 mice per cage. All behavioral tests were blinded to the genotype of mice and performed during the light phase between 09:00 and 17:00. Mice were

habituated to the testing rooms for 2 h before tests. All procedures for animal experiments were approved by the Institutional Animal Care and Use Committee of East China Normal University (ECNU).

Rt-PCR

Total RNA was extracted from brain tissues using TRNzol-A reagent (TIANGEN, Beijing, China) and then reversely transcribed to cDNA using the FastQuant RT kit (TIANGEN). An *Adamts18* cDNA fragment was amplified using the following primers: 5′-TCCTCATCT CACCGCTACCTCA-3′ (forward); and 5′-GGTCCCATCTTT GAACAGGCTA-3′ (reverse). A *β-actin* cDNA fragment was amplified as an internal control using the following primers: 5′-CCACCATGTACCCAGGCATT-3′ (forward) and 5′-AGGGTGTAAAACGCAGCTCA-3′ (reverse).

Quantitative real-time RT–PCR analysis

Quantitative real-time RT–PCR was performed using the StepOnePlus real-time PCR system (ThermoFisher, Carlsbad, CA, USA) with SuperReal PreMix Plus (SYBR Green; TIANGEN). Primers used in quantitative real-time RT–PCR are listed in Table 2. The relative quantity of target mRNA was determined using the $\Delta\Delta C_t$ method, with *Gapdh* as the reference gene. All reactions were performed in triplicates.

RNA in situ hybridization

RNA ISH was performed as described previously (Ataca et al., 2016). Briefly, mouse brains were fixed in 10% neutral buffered formalin for 24 h at RT and paraffin-embedded following the standard methods. ISH was performed on 5-μm-thick sections using the RNAscope 2.5 HD Reagent Kit-RED (Advanced Cell Diagnostics, Hayward, CA). *Adamts18* mRNA in mouse brains was detected by specific *Adamts18* probe. The sections were also hybridized with probe against mouse peptidylprolyl isomerase B (PPIB) or bacterial dihydrodipicolinate reductase (DapB) as positive and negative control, respectively.

Hematoxylin and eosin (HE) staining

Brain tissues were fixed in 10% neutral buffered formalin and embedded in paraffin. After dewaxing and rehydration, HE staining was performed on 5-μm sections following the standard protocol.

Nissl staining

For Nissl staining, 35-μm-thick frozen sections of mouse brains were prepared. The sections were immersed in Nissl staining solution (Beyotime Biotechnology, China) for 5 min, rinsed in distilled water twice for several seconds, and cleared in xylene twice for 10 min. Images were photographed with a microscope.

Immunofluorescence (IF) staining

For IF, 5-μm-thick paraffin-embedded brain sections were deparaffinized, rehydrated, and processed by microwave heating in sodium citrate-EDTA antigen retrieval solution. After washing with phosphate-buffered saline (PBS), sections were blocked with 3% BSA–PBS

for 1 h and then incubated with an appropriate antibody such as anti-microtubule-associated protein 2 (MAP2) and antilaminin overnight at 4 °C, followed by goat anti-rabbit IgG fluorescent secondary antibody (1:200) (Jackson Immuno Research, Cat. No. 111-165-003) for 1 h at RT. Then sections were washed with PBS and counterstained with 4′, 6-diamidino-2-phenylindole (DAPI) (MP Biomedicals, Cat. No.157574) 10 μg/ml in PBS. Finally, sections were mounted using antifade mounting medium (Beyotime Biotechnology, Cat. No. P0123) and images acquired by fluorescence microscope. An average of 12 sections was used to quantitate the IF intensity of MAP2 for each group. And there were at least 3 individual sex-matched mice in each group. Images were processed by being converted to gray scale after background subtraction in Image-Pro Plus 6.0 (IPP, MediaCybernetics, Inc., SilverSpring, MD, USA) software. The sum integrated optical density (IOD) and the sum areas were measured using IPP. Then mean fluorescence intensity was gained by dividing the sum area by the sum IOD.

Golgi staining

To examine morphologies of neurons and dendritic spines, Golgi staining was performed using the FD Rapid Golgi Stain Kit (FD Neurotechnologies, Baltimore, MD, USA). Briefly, quickly removed mice brains were immersed in the impregnation solution prepared in advance at room temperature (RT) for 2 weeks in the dark. After that, mice brains were transferred to another impregnation solution at RT for at least 72 h in the dark. Sections of 120 μm thick were cut on a cryostat (CM1900, Leica, Germany) at −20 °C followed by Golgi staining and mounting on gelatin-coated glass slides. Images were taken using a light microscope (Leica, Germany).

Analysis of dendritic morphology

To analyze dendritic morphologies of hippocampal dentate gyrus (DG) granule cells, measurements of total dendritic length and Sholl analysis of granule cells were performed using ImageJ 1.52d (National Institutes of Health, Bethesda, MD, USA; http://imagej.nih.gov/ij). Intact dendrites of granule cells were tracked by continuously adjusting the focal planes of the light microscope (Leica, Germany). A series of photographs of one neuron were composed by using the image sequence project of ImageJ followed by processing with the NeuronStudio software (version 0.9.92, Computational Neurobiology and Imaging Center, Mount Sinai School of Medicine, New York, NY, USA). Neurons were reconstructed by tracing with NeuronJ (a plugin of ImageJ), and the total dendritic lengths were automatically calculated by the software. Dendritic complexity was assessed by Sholl analysis (a plugin of ImageJ) on reconstructed neurons. 18 granule cells in DG were examined from each genotype group if the neurons were relatively isolated, easy to identify, and relatively intact with a complete dendritic tree.

Analysis of spine density

Spines on hippocampal DG granule cells were examined and imaged at 1000× magnification. Specific segments of spines on DG granule cells were reconstructed the same way as the analysis of dendritic morphology. The number of spines on a limited length of a dendrite was counted using the ImageJ software. At least three distal dendritic segments of

at least 15 μm in length, were analyzed per granule cell, and 9 granule cells each from WT mice and *Adamts18* KO littermates were examined.

Tail suspension test (TST)

For TST, mice were suspended by their tails with lab tape above the ground, in such a position that they cannot escape or hold on to nearby surfaces. Then total time that a mouse stayed immobile was recorded during the 6-min test.

Forced swim test (FST)

For FST, two clear glass cylinders (40 cm height × 20 cm diameter) were filled with water at room temperature (25 °C) to a height of 30 cm. A mouse was then placed in the water by holding its tail, and the time that the mouse stayed immobile before moving its head above the water was recorded by the software Any-maze during the 6-min test period.

Sucrose preference test

Mice were habituated to drinking water from two small bottles without any food restriction for the first 3 days. On the following 2 days, water in the two bottles was replaced by 1% (w/v) sucrose solution. The mice were single-housed and denied of water for 12 h. After that, each mouse was given one bottle of water and another bottle of 1% (w/v) sucrose solution in random order for 4 h. The total amount of water and 1% (w/v) sucrose solution consumed was regarded as the total intake, and sucrose preference (%) was expressed as the percentage of 1% (w/v) sucrose solution intake to the total intake.

Open-field test (OFT)

OFT was carried out to measure locomotor activity, anxiety-like behavior, and exploratory behavior. Each mouse was placed at the center of a defined open field (26 cm × 26 cm × 26 cm) and allowed to move freely in it for 15 min. The locomotor activity as indicated by the distance and speed of movements was monitored and recorded by a computerized video-tracking system equipped with the software Any-maze.

Elevated O maze

Elevated O maze was used to assess the anxiety level of mice. The apparatus has a circular platform (diameter 46 cm), which is elevated 46 cm above the floor. The circular platform is divided into 4 equal sectors of which two opposite sectors are double walled forming a channel between the two walls. The other 2 sectors, referred to as open sectors, are not walled. The test mouse was placed on one of the open sectors and allowed to freely explore for 5 min. The time that the mouse spent on open sectors was recorded by the software Any-maze (Stoelting, Wood Dale, IL, USA).

Light/dark transition test

The light/dark transition test was conducted to determine the anxiety level of mice. A cage (26 × 26 cm) was divided into two equal partitions (both 26 × 13 cm). One partition was brightly illuminated, and the other was dark. The test mouse was placed in the dark partition

and allowed to freely explore the two partitions for 15 min. The time that the mouse spent in the light partition was recorded by the software Truscan 2.01.

Three chamber test

The three chamber test was performed to assess the sociability and social novelty of mice. The apparatus consists of a transparent acrylic box (60 × 40 cm) that is divided equally into three chambers (20 × 40 cm each). Each chamber has a door (8 × 6 cm). Two age-matched stranger mice (Stranger 1 and Stranger 2) that had no prior contact with the test mouse were habituated by placing them separately in the two lateral chambers for 25 min a day for 3 days prior to testing. On the test day, the test mouse was placed in the middle chamber and allowed to explore all three chambers for 10 min. The test mouse was then put back in the middle chamber and denied access to the other 2 chambers. Stranger 1 mouse was then placed in one of the two lateral chambers, and the test mouse was allowed to freely explore all three chambers for 10 min to become familiar with Stranger 1. For the social novelty test, Stranger 2 was introduced into the previously empty chamber, and the test mouse was allowed to explore all three chambers for 10 min. The time the test mouse spent in each chamber was recorded by the software Any-maze (Stoelting, Wood Dale, IL, USA).

Novel object recognition

Novel object recognition was used to evaluate the short-term memory of mice. Mice were habituated 5 min a day for 3 consecutive days in a box (29 × 29 × 25 cm). On the final day, the test mouse was placed in the box containing two identical objects (A and B) for 8 min. One hour later, one of the two identical objects was replaced by a novel object (object C), and the test mouse was permitted to explore the box for 5 min. Mice were supposed to interact more with the novel object. The objects were washed with 70% alcohol between tests.

Radial eight-arm maze (RAM) test

RAM test was conducted to assess the spatial learning ability and working memory of mice. RAM consists of a central platform (diameter 25 cm) with eight radiating arms. Each arm is shielded with 15-cm-high walls and has a small plastic food cup at the end. The maze is positioned 1 m above ground, and a camera is placed above the maze. Mice were individually housed and restricted for food until their body weight was reduced to approximately 85% of the original body weight. During the first two days, mice were habituated 10 min a day for finding food on each arm. In the next three days, each mouse was individually trained to find food on the maze with only one arm containing food until 10 min or food was found. 2 trials were performed each day. On the test day, all arms were baited, and the time required for the mouse to find all baits and the number of arms each mouse visited were recorded. The test was terminated when all food baits were found or when 10 min had elapsed. Re-entry into the previously visited arms was considered an error. Error % (number of errors/number of arms each mouse visited) was used to assess the performance of mice in RAM.

Morris water maze (MWM) test

The MWM test was used to assess the spatial learning ability of mice. MWM consists of a circular pool that is filled half-way with water. A platform is placed somewhere in the pool with its top approximately one inch above water. A camera with tracking system is placed above the pool. The circular pool is equally divided into four quadrants by two lines. The ends of the lines demarcate four starting points (points 1, 2, 3, 4) on the pool rim for swimming. During the training phase, each mouse was given 4 swimming trials per day for 4 days with random starting points, and each trial was terminated when the mouse found the platform or 1 min had elapsed. If the mouse failed to find the platform within 1 min, it was guided to the platform and allowed to rest on it for ~30 s. On the 5th day (the test day), the platform was submerged in water, and the time required for the mouse to find the platform from each of the starting point was recorded.

Sandwich ELISA and Western blotting

For Sandwich ELISA, brain tissues were dissected from mice, weighted, and homogenized in 0.1 M PBS buffer (pH 7.4) containing protease inhibitor cocktail at 1 g/10 mL at 4 °C. After centrifugation at 12,000*g* for 10 min, laminin levels were measured, according to the manufacturer's instructions of the ELISA kit (LYBD Bio-Technique Co, Ltd, Beijing, China). For Western blot, brain tissues were dissected from mice, weighted, and homogenized in RIPA buffer [50 mM Tris (pH7.4), 150 mM Nacl, 1% Triton X-100, 1% sodium deoxycholate, 0.1% SDS] (Boster Wuhan, China), with protease inhibitors and phosphatase inhibitors (Roche, Basel, Switzerland). The samples were centrifuged at 12,000 rpm for 15 min at 4 °C and tissue debris was removed. Protein concentration was determined by BCA assay reagent (Pierce, Rockford, IL, USA). Proteins were separated on a 12% SDS–PAGE under reducing conditions and then transferred onto a polyvinylidene difluoride (PVDF) membrane. The membrane was blocked in blocking buffer (PBS, 0.5% Tween-20, and 5% non-fat dry milk powder) and then incubated with primary antibody for 1 h at RT. After washing, the membrane was incubated with horseradish peroxidase (HRP)-conjugated secondary antibody for 1 h at RT. The immunoreactive bands were visualized with enhanced chemiluminescence (ECL) Western blot kit (Millipore, Boston, MA, USA), and quantified using ImageJ version 1.50i.

Statistical analysis

All data are presented as mean ± SEM. Data were analyzed using two-tailed unpaired student's *t*-test or analysis of variance (ANOVA). Kolmogorov–Smirnov's test was used for the Sholl analysis of dendritic complexity. For RAM test, error% was analyzed using repeated measures of ANOVA to determine genotype effects on behavioral responses. For the MWM test, the learning curves (latency during the training phase) of mice were analyzed using repeated measures ANOVA. Differences were considered significant if $P < 0.05$.

RESULTS

Expression of *Adamts18* mRNA in mouse brain

To clarify the potential roles of ADAMTS18 in CNS, we determined *Adamts18* mRNA levels in mouse brains at different developmental stages. RT–PCR analyses showed that *Adamts18* mRNA levels were very high in the brains of embryos (E18.5) and two-week-old mice, but were significantly decreased in adult (15 weeks) brains (Fig. 1A, B). In situ hybridization revealed that *Adamts18* mRNAs were present in most areas of the brain of two-week-old mice, especially in the granular cell layer of cerebellum and the hippocampus DG granular cell layer (Fig. 1C, D); however, the abundance of *Adamts18* mRNAs was dramatically decreased in the corresponding areas of adult brains (Fig. 1D).

ADAMTS18 deficiency has little effect on gross anatomy of the brain

The gross anatomy of the brain was then examined, and no apparent abnormalities were found in the brains of *Adamts18* KO mice and their WT littermates (Fig. 2A). Nissl staining revealed no gross structure alterations in the whole brain (Fig. 2B) and the six neural cell layers (Fig. 2C) in the cerebral cortex of *Adamts18* KO mice. The numbers of hematoxylin-positive cells in cerebral cortex, hippocampus, and cerebellum in *Adamts18* KO mice were similar to those in WT mice (Fig. 2D, E).

ADAMTS18 deficiency leads to alteration in dendritic structural plasticity in DG granule cells

We further determined the numbers of dendrites and axons in adult mouse brain sections. IF staining showed that the MAP2 (a dendrite marker) mean intensity was higher in *Adamts18* KO mice than in WT mice (1.723 ± 0.07734 vs. 1.425 ± 0.002959, $*P < 0.05$) (Fig. 3A, B), indicating that there was a higher density of DG dendrites in *Adamts18* KO mice. However, there were no significant difference in axon numbers, determined by anti-Tau-1 (an axon marker) staining, between *Adamts18* KO mice and their WT littermates (data not shown). Golgi staining of brain sections was then performed to examine morphological alterations in DG granule cells. Increased numbers of stained granule cells with more neurites were consistently observed in *Adamts18* KO mice compared with WT mice (Fig. 3C). Furthermore, a marked increase in average total dendritic length (1110 ± 91.02 μm vs. 870.3 ± 65.64 μm, $*P < 0.05$) (Fig. 3D) of DG granule cells was seen in *Adamts18* KO mice. Sholl analysis of reconstructed dendrites (Fig. 3E) revealed that dendritic arborization (or dendritic branching) was increased in *Adamts18* KO mice compared to WT mice (Fig. 3F). The number of dendritic spines on DG granule cells was also significantly increased in *Adamts18* KO mice compared with WT mice (9.919 ± 0.285 per 10 μm vs. 8.811 ± 0.372 per 10 μm, $*P < 0.05$) (Fig. 3G–I). Since the postsynaptic density 95 (PSD-95) is a key protein that maintains spine stability (Ehrlich et al., 2007; Lambert et al., 2017), its level in hippocampus was determined by Western blotting. Results showed that the levels of PSD-95 were significantly higher in *Adamts18* KO mice than in WT mice (Fig. 3J, K). These results suggest a role of ADAMTS18 in the maintenance of dendritic structural plasticity of DG granule cells.

ADAMTS18 deficiency reduces depression-like behaviors in mice

A battery of behavioral tests was then performed (Table 3). In the OFT, *Adamts18* KO mice traveled a longer distance (3589 ± 192.6 cm vs. 3019 ± 176.7 cm) than their WT littermates (**P* < 0.05) (Fig. 4A), suggesting that *Adamts18* KO mice have higher levels of spontaneous activities than WT mice. The central distance over the total distance (39 ± 1.5% vs. 32 ± 1.7%), time spent in the central area (46 ± 2.1 % vs. 37 ± 2.5%), and entries to the center area (126 ± 8.7 times vs. 102 ± 6.1 times) were all significantly increased in *Adamts18* KO mice compared to their WT littermates (Fig. 4B–D), suggesting that *Adamts18* KO mice had lower anxiety levels than their WT littermates. In the TST, *Adamts18* KO mice had a decreased immobility time compared with their WT littermates (201 ± 14.9 vs. 242 ± 7.3 s, **P* < 0.05) (Fig. 4E). In the FST, the immobility time was significantly reduced in *Adamts18* KO mice (66 ± 8.4 vs. 93 ± 8.6 s, **P* < 0.05) (Fig. 4F), suggesting *Adamts18* KO mice have significantly reduced levels of depression-like reactions. To exclude the influence of hyperactivity of KO mice, we performed sucrose preference test, which is a classic method for investigating anhedonia of mice. *Adamts18* KO mice were found to have higher sucrose preference (%) than their WT littermates (68 ± 3.1 vs. 57 ± 2.8, **P* < 0.05) (Fig. 4G).

ADAMTS18 deficiency leads to activation of the laminin/PI3K/AKT/GSK-3β/CRMP2 signaling pathway in embryonic brain

We previously showed that ADAMTS18 deficiency influences the early adipocyte directional differentiation associated with increased laminin expression (Zhu et al., 2018). As laminin is also crucial for neuronal polarity (Esch et al., 1999; Menager et al., 2004), we wonder whether *Adamts18* deficiency affects the neurite morphologies in association with laminin. IHC (Fig. 5A) was first performed to examine the distribution of laminin in the brain; results showed that laminin levels were significantly increased in embryonic brains (E14.5) of *Adamts18* KO mice compared to their WT littermates. Sandwich ELISA of brain tissue (Fig. 5B) showed that *Adamts18* KO brain had a higher amount of laminin than the WT (458.4 ± 27.1 ng/mg vs. 402 ± 39.9 ng/mg). qRT-PCR was then performed to measure mRNA levels of various laminin subunits including *laminin α1*, *3*, *5*, *β1*, and *γ1*. Results showed that the mRNA levels of *laminin α5*/*β1* were significantly increased in embryonic brain of *Adamts18* KO mice compared to those of their WT littermates (Fig. 5C, D). No significant difference was observed for other laminin subunits (such as *laminin α3*, *5*, and *γ1*) between WT and *Adamts18* KO mice (Data not shown). The role of the laminin-mediated phosphatidylinositol 3-kinase (PI3-kinase)/Akt/glycogen synthasekinase-3β (GSK-3β)/collapsin response mediator protein-2 (PI3K/AKT/GSK-3β/CRMP2) signaling pathway in the regulation of neuron polarization was then investigated (Inagaki et al., 2001; Yoshimura et al., 2005). Although non-phosphorylated forms of these proteins showed no significant differences in embryonic brain, protein levels of phospho-PI3K (Tyr^{458}), phospho-AKT (Ser^{473}), and phosphor-GSK-3β (Ser^{9}) were significantly increased and those of phosphorylated CRMP2 (Thr^{514}) were decreased in embryonic brains of *Adamts18* KO mice compared to their WT controls (Fig. 5E, F). These results suggest that ADAMTS18 deficiency leads to activation of the laminin/PI3K/AKT/GSK-3β/CRMP2 signaling pathway in embryonic brains (Fig. 5G).

ADAMTS18 deficiency alters the transcription levels of other *ADAMTS* genes in embryonic brains

Since some ADAMTSs (e.g. ADAMTS-1, 4, 5, and 9) have been reported to be involved in neurite outgrowth and synaptic plasticity (Lemarchant et al., 2013; Gottschall and Howell, 2015), the possibility that *Adamts18* deletion affects the expression of other ADAMTS family members was determined. qRT-PCR was performed to measure the amounts of *Adamts1*, *3*, *4*, *5*, *9*, *16* mRNA (Fig. 6A–F), and only the levels of *Adamts1* mRNA was found to be significantly increased in the brain of *Adamts18* KO mice (Fig. 6A). These data suggest that *Adamts18* deletion could affect the expression of other *Adamts* genes; this may be a compensatory effect for *Adamts18* deletion.

DISCUSSION

In this study, we investigated the cellular and behavioral phenotypes of *Adamts18* KO mice. Our study demonstrates that ADAMTS18 plays a critical role in neuronal morphogenesis and control of emotional reactions in mice.

Adamts18 was found to be highly expressed in the hippocampus DG granular cell layer of developing (embryonic) brains (Fig. 1D), suggesting that ADAMTS18 plays an important role in the development of neurons in this region. This possibility was corroborated by the observation that *Adamts18* KO mice displayed higher dendritic branching complexity and spine density on hippocampal DG granular cells (Fig. 3). Our data also showed that ADAMTS18 deficiency leads to increased laminin expression in embryonic mouse brains (Fig. 5). Laminin is a major ECM component of the basal lamina (Tunggal et al., 2000); it induces rapid production of phosphatidylinositol 3, 4, 5-triphosphate (PIP_3) at the tip of a neurite through the action of PI3-kinase (Esch et al., 1999; Menager et al., 2004). PIP_3 then activates Akt by phosphorylation at Thr-308/Ser-473; activated Akt phosphorylates GSK-3β at Ser-9 and inactivates its kinase activity. Inactivated GSK-3β (phosphorylated form) loses its ability to phosphorylate CRMP2 at Thr-514/Ser-518, leading to increased levels of nonphosphorylate CRMP2 (activated CRMP2). CRMP2 is mainly located in axon, dendrite, growth cone, and neuronal cell body. In embryo, it regulates neurite growth. Many studies have shown that the increase in activated CRMP2 induces multiple neurite formations (Inagaki et al., 2001; Yoshimura et al., 2005). In line with this view, our data demonstrated that this signaling pathway was markedly enhanced in the embryonic brain of *Adamts18* KO mice (Fig. 5E–G), suggesting activated laminin/PI3K/AKT/GS K-3β/CRMP2 signaling pathway is one of the possibilities to induce increased dendritic branching complexity as observed in *Adamts18* KO mice (Fig. 3). In addition, the upregulation in the expression of laminin subunit *Lama5* in embryonic brain of *Adamts18* KO mice (Fig. 5C) could contribute to this phenomenon. It has been shown that *Lama5* mRNA is highly abundant in the hippocampal DG (Omar et al., 2017) and is largely overlapped with *Adamts18*. As laminin α5 is a stabilizer of dendritic spines and synapses (Omar et al., 2017), it is possible that ADAMTS18 modulates dendritic spine stability by regulating the production of laminin α5. The expression of PSD-95 protein was also significantly increased in *Adamts18* KO mice (Fig. 3J, K). PSD-95 has also been shown to play a vital role in maintaining spine stability.

Therefore, it is likely that ADAMTS18 affects spine stability partly through regulating the expression of laminin α5 and PSD-95 in granule cells.

At the molecular level, ADAMTS18 may also cleave ECM components or regulates other signaling pathways. Several studies have reported that some ADAMTS family members are involved in embryonic brain development by degrading the ECM. ADAMTS3 is expressed in the excitatory neurons of the embryonic and postnatal cerebral cortex and hippocampus. Ogino et al. (2017) reported that ADAMTS3 inactivates Reelin in the cerebral cortex and hippocampus by cleaving it at Reelin repeat 3 (N-t site). Reelin is a secreted glycoprotein and is essential for embryonic brain development and adult brain functions. Conditional KO mice, in which ADAMTS3 is deficient only in the excitatory neurons of the forebrain, show increased dendritic branching and elongation in the postnatal cerebral cortex (Ogino et al., 2017). ADAMTS4 (Hisanaga et al., 2012) and ADAMTS5 (Krstic et al., 2012) also mediate N-t cleavage, but whether they cleave Reelin *in vivo* has not been investigated. In this study, we detected the association of ADAMTS18 with other ADAMTSs (ADAMTS1, 3, 4, 5, 9, and 16) in embryonic stage (Fig. 6). Only the levels of *Adamts1* mRNA were found to be significantly increased in the brain of *Adamts18* KO mice. ADAMTS1 has been found to be expressed in the mouse and rat brain during development (Thai and Iruela-Arispe, 2002; Gunther et al., 2005). ADAMTS1 expression is closely associated with an increase in the ADAMTS-specific N-terminal cleavage fragment of brevican (Yuan et al., 2002). We therefore hypothesize that ADAMTS18 can affect mouse phenotypes through degrading some important ligands or extracellular matrices. Further study will clarify the role of ADAMTS18 in this aspect.

The elaborate structure of the dendritic arbor is a hallmark of neurons. It is a major defining factor of how input information is integrated and how synaptic plasticity is maintained (Hausser et al., 2000; Jan and Jan, 2010). Changes in dendritic structure have been observed in multiple psychiatric disorders, including depression (Qiao et al., 2016). Hippocampus is the most well-studied brain region in depression research because it is part of the limbic system with nerve fiber connecting emotion-related brain regions including the prefrontal cortex and amygdala. It has been shown that changes in hippocampal dendritic structure, such as dendritic branching complexity and spine density, are closely related to depression (Qiao et al., 2016). In this study, we found that *Adamts18* KO mice showed reduced levels of depression-like reactions (Fig. 4E–G). This could be attributed in part to increased dendritic branching complexity and spine density of hippocampal DG granular cells in *Adamts18* KO mice. In future studies, we will further evaluate the reduction in depression-like behaviors in *Adamts18* KO mice using several chronic stress models, such as chronic restraint stress (CRS), chronic unpredictable mild stress (CUMS), and chronic social defeat stress (CSDS).

ADAMTS18 was previously linked to white matter integrity in healthy 72- to 74-year-old people by a genome-wide association study (Lopez et al., 2012). In this study, we examined the gross anatomy of the brains of *Adamts18* KO mice using Nissl staining and H&E staining (Fig. 2) and no abnormalities in the white matter. This finding is contradictory to those of previously reported. We attribute this discrepancy to age difference. More studies are needed to find out the changes in the white matter of older *Adamts18* KO mice. In

summary, our findings indicate that ADAMTS18 plays an important role in neuronal morphogenesis and emotional control in CNS. Since the regulation of brain development is a complex process and involves a large number of molecules, further studies are required to identify ADAMTS18′s substrates, intermolecular interactions, or other signaling networks.

ACKNOWLEDGMENTS

This work was supported by grants from the National Science Foundation of China (No. 81570389 and No. 81770139 to Wei Zhang; No. 81200352 to Suying Dang) and Shanghai Municipal Natural Science Foundation (16ZR1423700 to Suying Dang). We thank Dr. Chao-Hung Lee for editing the manuscript and providing valuable advices.

Abbreviations:

CNS	central nervous system
CRMP2	collapsin response mediator protein-2
DAPI	4′, 6-diamidino-2-phenylindole
DG	dentate gyrus
FST	forced swim test
HE	hematoxylin and eosin
IF	immunofluorescence
IPP	Image-Pro Plus
ISH	in situ hybridization
KO	knockout
MWM	Morris water maze
OFT	open field test
PBS	phosphate-buffered saline
PIP_3	phosphatidylinositol 3, 4, 5-triphosphate
RAM	radial eight-arm maze
SNPs	single-nucleotide polymorphisms
TST	tail suspension test
WT	wild type

REFERENCES

Aldahmesh MA, Alshammari MJ, Khan AO, Mohamed JY, Alhabib FA, Alkuraya FS (2013) The syndrome of microcornea, myopic chorioretinal atrophy, and telecanthus (mmcat) is caused by mutations in adamts18. Hum Mutat 34:1195–1199. [PubMed: 23818446]

Aldahmesh MA, Khan AO, Mohamed JY, Alkuraya H, Ahmed H, Bobis S, Al-Mesfer S, Alkuraya FS (2011) Identification of adamts18 as a gene mutated in knobloch syndrome. J Med Genet 48:597–601. [PubMed: 21862674]

Apte SS (2009) A disintegrin-like and metalloprotease (reprolysintype) with thrombospondin type 1 motif (adamts) superfamily: functions and mechanisms. J Biol Chem 284:31493–31497. [PubMed: 19734141]

Ataca D, Caikovski M, Piersigilli A, Moulin A, Benarafa C, Earp SE, Guri Y, Kostic C, et al. (2016) Adamts18 deletion results in distinct developmental defects and provides a model for congenital disorders of lens, lung, and female reproductive tract development. Biol Open 5:1585–1594. [PubMed: 27638769]

Ehrlich I, Klein M, Rumpel S, Malinow R (2007) Psd-95 is required for activity-driven synapse stabilization. Proc Natl Acad Sci U S A 104:4176–4181. [PubMed: 17360496]

Esch T, Lemmon V, Banker G (1999) Local presentation of substrate molecules directs axon specification by cultured hippocampal neurons. J Neurosci 19:6417–6426. [PubMed: 10414970]

Gottschall PE, Howell MD (2015) Adamts expression and function in central nervous system injury and disorders. Matrix Biol 44–46:70–76.

Gunther W, Skaftnesmo KO, Arnold H, Bjerkvig R, Terzis AJ (2005) Distribution patterns of the anti-angiogenic protein ADAMTS-1 during rat development. Acta Histochem 107:121–131. [PubMed: 15878613]

Hausser M, Spruston N, Stuart GJ (2000) Diversity and dynamics of dendritic signaling. Science 290:739–744. [PubMed: 11052929]

Hisanaga A, Morishita S, Suzuki K, Sasaki K, Koie M, Kohno T, Hattori M (2012) A disintegrin and metalloproteinase with thrombospondin motifs 4 (ADAMTS-4) cleaves Reelin in an isoform-dependent manner. FEBS Lett 586:3349–3353. [PubMed: 22819337]

Inagaki N, Chihara K, Arimura N, Menager C, Kawano Y, Matsuo N, Nishimura T, Amano M, et al. (2001) Crmp-2 induces axons in cultured hippocampal neurons. Nat Neurosci 4:781–782. [PubMed: 11477421]

Jan YN, Jan LY (2010) Branching out: mechanisms of dendritic arborization. Nat Rev Neurosci 11:316–328. [PubMed: 20404840]

Jin H, Wang X, Ying J, Wong AH, Li H, Lee KY, Srivastava G, Chan AT, et al. (2007) Epigenetic identification of adamts18 as a novel 16q23.1 tumor suppressor frequently silenced in esophageal, nasopharyngeal and multiple other carcinomas. Oncogene 26:7490–7498. [PubMed: 17546048]

Kelwick R, Desanlis I, Wheeler GN, Edwards DR (2015) The adamts (a disintegrin and metalloproteinase with thrombospondin motifs) family. Genome Biol 16:113. [PubMed: 26025392]

Krstic D, Rodriguez M, Knuesel I (2012) Regulated proteolytic processing of reelin through interplay of tissue plasminogen activator (tpa), adamts-4, adamts-5, and their modulators. PLoS One 7 e47793. [PubMed: 23082219]

Lambert JT, Hill TC, Park DK, Culp JH, Zito K (2017) Protracted and asynchronous accumulation of psd95-family maguks during maturation of nascent dendritic spines. Dev Neurobiol 77:1161–1174. [PubMed: 28388013]

Lemarchant S, Pruvost M, Montaner J, Emery E, Vivien D, Kanninen K, Koistinaho J (2013) Adamts proteoglycanases in the physiological and pathological central nervous system. J Neuroinflammation 10:133. [PubMed: 24176075]

Lopez LM, Bastin ME, Maniega SM, Penke L, Davies G, Christoforou A, Valdes Hernandez MC, Royle NA, et al. (2012) A genome-wide search for genetic influences and biological pathways related to the brain's white matter integrity. Neurobiol Aging 33(1847): e1841–1814.

Lu T, Dang S, Zhu R, Wang Y, Nie Z, Hong T, Zhang W (2017) Adamts18 deficiency promotes colon carcinogenesis by enhancing beta-catenin and p38mapk/erk1/2 signaling in the mouse model of aom/dss-induced colitis-associated colorectal cancer. Oncotarget. 10.18632/oncotarget.14866.

Menager C, Arimura N, Fukata Y, Kaibuchi K (2004) Pip3 is involved in neuronal polarization and axon formation. J Neurochem 89:109–118. [PubMed: 15030394]

Ogino H, Hisanaga A, Kohno T, Kondo Y, Okumura K, Kamei T, Sato T, Asahara H, et al. (2017) Secreted metalloproteinase ADAMTS3 inactivates reelin. J Neurosci 37:3181–3191. [PubMed: 28213441]

Omar MH, Kerrisk Campbell M, Xiao X, Zhong Q, Brunken WJ, Miner JH, Greer CA, Koleske AJ (2017) Cns neurons deposit laminin alpha5 to stabilize synapses. Cell Rep 21:1281–1292. [PubMed: 29091766]

Peluso I, Conte I, Testa F, Dharmalingam G, Pizzo M, Collin RW, Meola N, Barbato S, et al. (2013) The adamts18 gene is responsible for autosomal recessive early onset severe retinal dystrophy. Orphanet J Rare Dis 8:1–8. [PubMed: 23286897]

Porter S, Clark IM, Kevorkian L, Edwards DR (2005) The adamts metalloproteinases. Biochem J 386:15–27. [PubMed: 15554875]

Qiao H, Li MX, Xu C, Chen HB, An SC, Ma XM (2016) Dendritic spines in depression: what we learned from animal models. Neural Plast 2016:8056370. [PubMed: 26881133]

Thai SN, Iruela-Arispe ML (2002) Expression of ADAMTS1 during murine development. Mech Dev 115:181–185. [PubMed: 12049787]

Tunggal P, Smyth N, Paulsson M, Ott MC (2000) Laminins: structure and genetic regulation. Microsc Res Tech 51:214–227. [PubMed: 11054872]

Wei J, Liu CJ, Li Z (2014) Adamts-18: a metalloproteinase with multiple functions. Front Biosci (Landmark Ed) 19:1456–1467. [PubMed: 24896365]

Xiong DH, Liu XG, Guo YF, Tan LJ, Wang L, Sha BY, Tang ZH, Pan F, et al. (2009) Genome-wide association and follow-up replication studies identified adamts18 and tgfbr3 as bone mass candidate genes in different ethnic groups. Am J Hum Genet 84:388–398. [PubMed: 19249006]

Yoshimura T, Kawano Y, Arimura N, Kawabata S, Kikuchi A, Kaibuchi K (2005) Gsk-3beta regulates phosphorylation of crmp-2 and neuronal polarity. Cell 120:137–149. [PubMed: 15652488]

Yuan W, Matthews RT, Sandy JD, Gottschall PE (2002) Association between protease-specific proteolytic cleavage of brevican and synaptic loss in the dentate gyrus of kainate-treated rats. Neuroscience 114:1091–1101. [PubMed: 12379262]

Zhu R, Cheng M, Lu T, Yang N, Ye S, Pan YH, Hong T, Dang S, et al. (2018) A disintegrin and metalloproteinase with thrombospondin motifs 18 deficiency leads to visceral adiposity and associated metabolic syndrome in mice. Am J Pathol 188:461–473. [PubMed: 29169989]

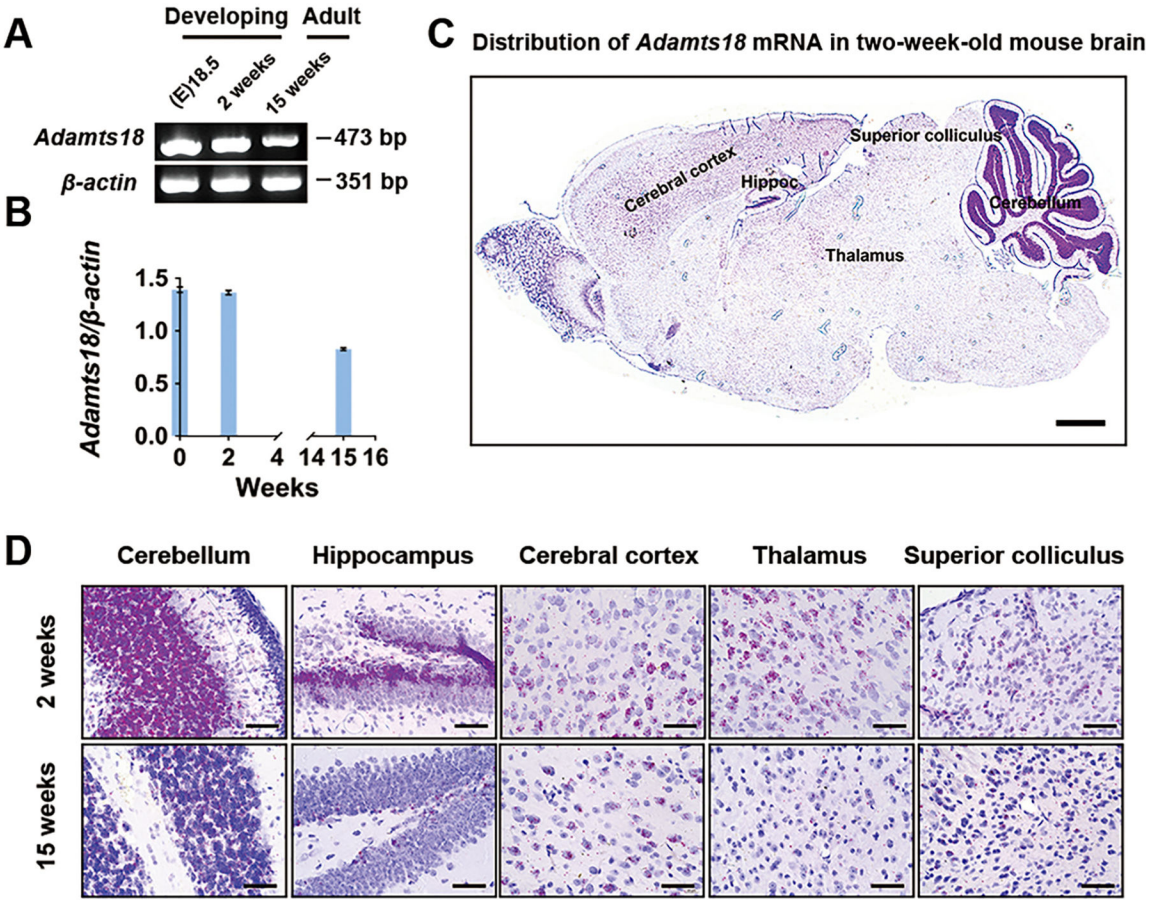

Fig. 1.

Spatio-temporal expression of *Adamts18* mRNA in mouse brains. (A) Relative expression levels of *Adamts18* mRNA were detected by RT–PCR in brains of wild-type C57BL/6/129Sv mice at different development stages, including embryonic (E) 18.5, 2 weeks postnatal, and adult (15 weeks postnatal). *β-actin* mRNA was assessed as internal reference. (B) Quantification of *Adamts18* mRNA expression in mouse brains at different development stages. (C) *In situ* hybridization (ISH) of *Adamts18* mRNA in wild-type mouse brains (sagittal tissue section). ISH-positive signals are shown as pink dots in cells. Scale bar, 15 mm. (D) ISH of *Adamts18* mRNA in various brain areas (sagittal tissue section) of two-week-old mice (upper panel) and fifteen-week-old mice (lower panel). Scale bar, 50 μm.

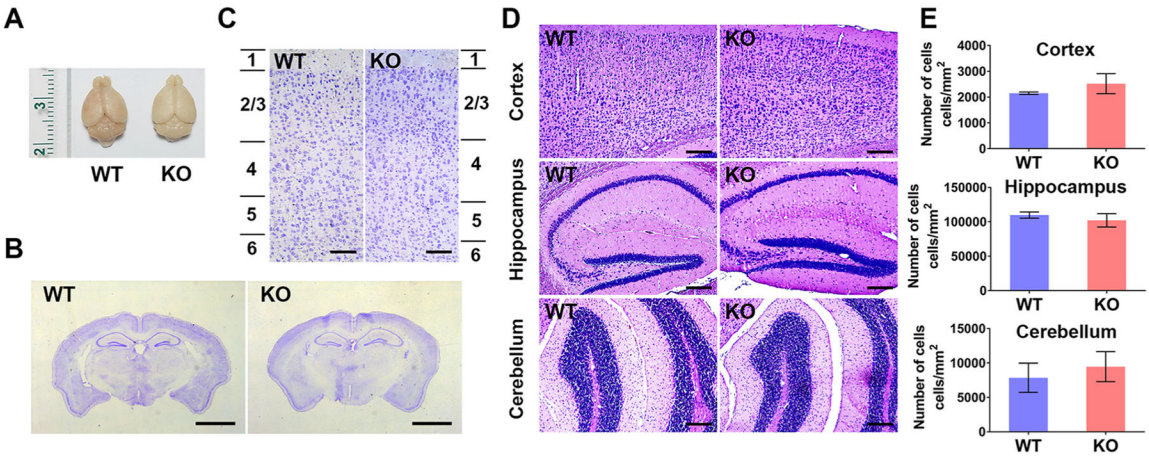

Fig. 2.

No effects of ADAMTS18 deficiency on adult brain structure and number of nerve cells in various brain areas. (A) Representative images of the whole brains of *Adamts18* KO mice and their WT littermates at adult stage (8 weeks). (B) Brain anatomy of *Adamts18* KO mice and their WT littermates shown by Nissl staining. Scale bar, 2 mm. (C) Cortical lamination of *Adamts18* KO mice and their WT littermates revealed by Nissl staining in sagittal tissue sections. Scale bar, 200 mm. 1, Molecular layer; 2/3, External granular cell layer/external pyramidal cell layer; 4, Internal granular cell layer; 5, Internal pyramidal cell layer; 6, multiform layer. (D) Brain cells detected by hematoxylin–eosin (HE) staining in cortex (upper panel), hippocampus (middle panel), and cerebellum (bottom panel) of the brains of adult *Adamts18* KO mice and their WT littermates (sagittal tissue sections). Scale bar, 100 μm. (E) Quantification of brain cells in cortex (upper), hippocampus (middle) and cerebellum (bottom) in adult *Adamts18* KO mice and their WT littermates (n = 4/group). Bars indicate mean ± SEM.

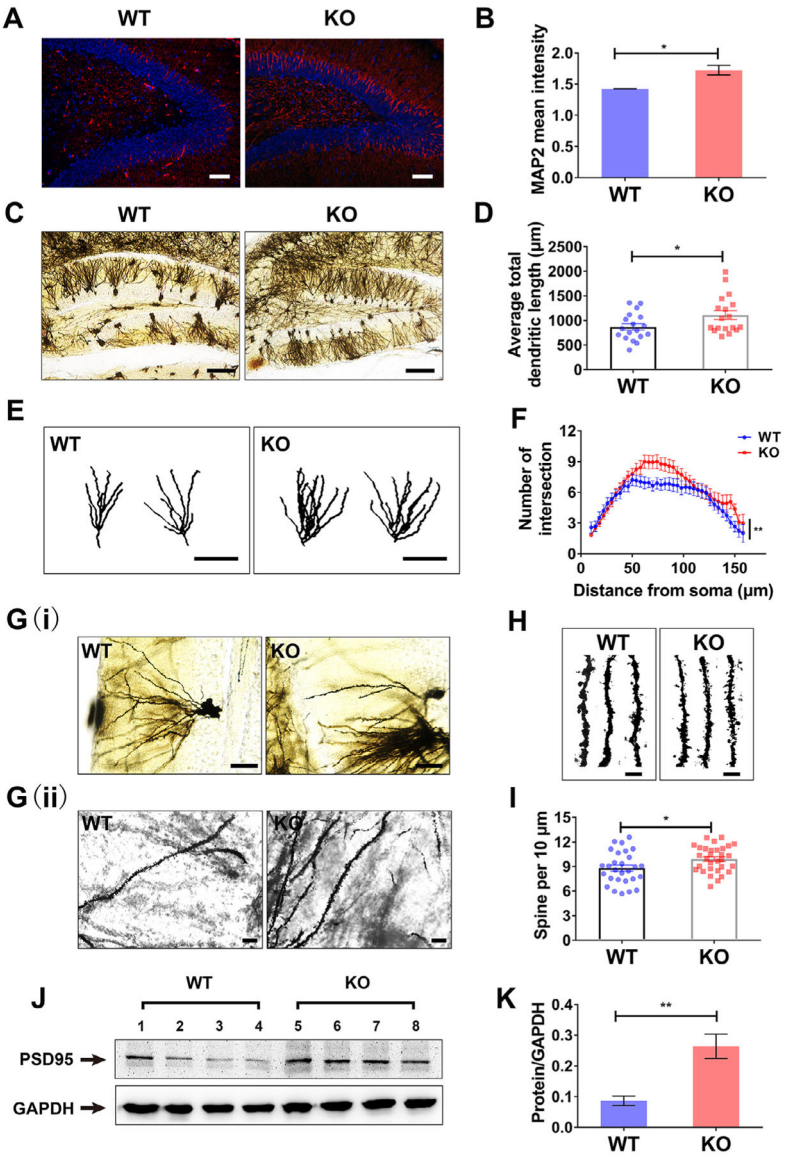

Fig. 3.

Effect of ADAMTS18 deficiency on dendritic density and structural plasticity of dendrites in hippocampal dentate gyrus granule cells. (A) Representative results of immunofluorescence staining for microtubule-associated protein 2 (MAP2) (a dendrite marker) in hippocampal dentate gyrus of mice. Red, MAP2 staining; blue, DAPI (4′, 6-diamidino-2-phenylindole) staining, Scale bar = 50 μm. (B) Quantification of MAP2 mean intensity (n = 3/group). (C) Representative images of Golgi staining of hippocampal dentate gyrus granule cells from different genotypes of mice. Scale bar = 200 μm. (D) Quantification of total dendritic length of granule cells in hippocampal dentate gyrus of mice. Data were derived from 18 granule cells each from *Adamts18* KO mice and WT littermates. (E) Representative images of reconstructed dendritic arbors from different genotypes of littermates (n = 3/group). Scale bar = 100 μm. (F) Dendritic complexity of granule cells in hippocampus determined by Sholl analysis. (G) Representative images of dendritic spines on hippocampal granule cells

at 400× magnification (i) or 1000× magnification (ii). (H) Representative images of dendritic spines of WT and KO mice. (I) Quantification of dendritic spine density. (J) Protein level of PSD-95 in hippocampus from adult mice determined by Western blotting. GAPDH was used as the loading control. (K) Quantification of PSD-95 protein levels. Data are presented as mean ± SEM. Kolmogorov–Smirnov's test was used for the Sholl analysis of dendritic complexity. $*P < 0.05$, $**P < 0.01$. These experiments were repeated independently at least three times.

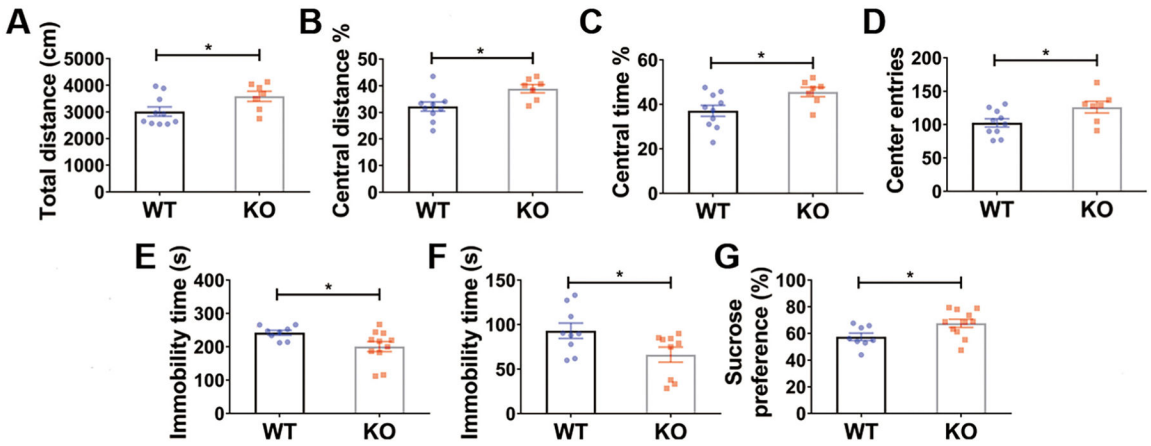

Fig. 4.

Increased spontaneous activity, and reduced depression- and anxiety-like reactions in *Adamts18* KO mice. Locomotor activity of WT mice ($n = 12$) and *Adamts18* KO mice ($n = 8$) were measured by the open field. (A) WT mice traveled a shorter distance than *Adamts18* KO mice. (B) The central distance over the total distance of WT mice was significantly lower than that of *Adamts18* KO mice. (C) WT mice spent less time in the central area than *Adamts18* KO mice. (D) *Adamts18* KO mice made more entries to the center area than their WT littermates. (E) Immobility time in the Tail Suspension Test of WT mice ($n = 8$) and *Adamts18* KO mice ($n = 11$). (F) Immobility time during the last 4 min of the 6-minute testing period in the Forced Swim Test of WT mice ($n = 9$) and *Adamts18* KO mice ($n = 9$). (G) Sucrose preference % (Sucrose solution consumption/Total liquid consumption*100%) of WT ($n = 8$) and *Adamts18* KO mice ($n = 11$). Data are presented as mean ± SEM. Statistically significant differences were determined by student *t* test. $^{*}P < 0.05$.

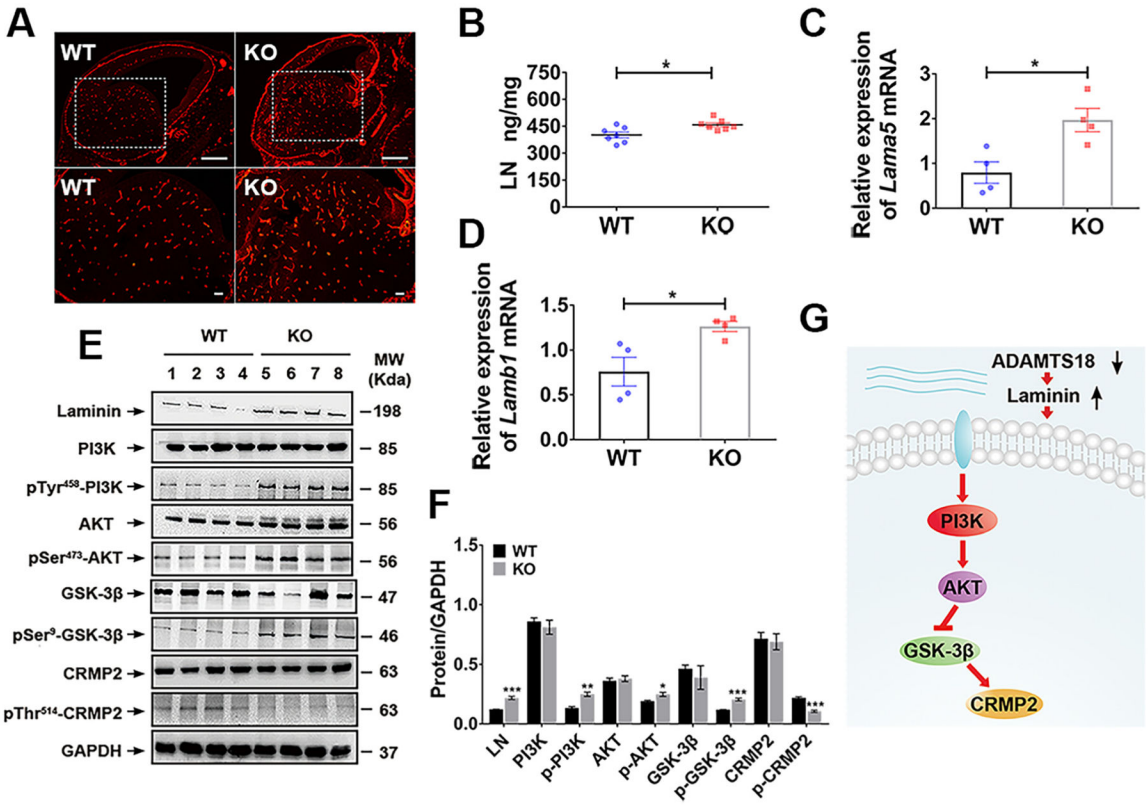

Fig. 5.

Activated PI3K/Akt/GSK-3/CRMP2 pathway in embryonic brains of *Adamts18* KO mice. (A) Laminin (LN) immunohistochemistry staining of E14.5 mouse brain. Scale bar, 500 μm (top panel) and 50 μm (bottom panel). (B) Expressions of LN in embryonic mouse brains determined by sandwich ELISA. Each symbol represents one mouse. Horizontal bars represent mean value ($n = 7$/group). (C, D) Relative mRNA levels of *laminin α5* (C) and *laminin β1* (D) in E14.5 mouse brains determined by quantitative real-time RT–PCR. The relative quantity of target gene was normalized to housekeeping gene *Gapdh* using the $\Delta\Delta C_t$ method. Data are expressed as mean ± SEM. (E, F) Activated PI3K/Akt/GSK-3/CRMP2 pathway in embryonic brains of *Adamts18* KO mice determined by Western blotting (E); the bar graph (F) shows relative levels of the proteins as mean ± SEM. GAPDH was used as the loading control. (G) Cartoon picture shows that ADAMTS18 deficiency in the E14.5 brain activates extracellular laminin-mediated PI3/Akt/GSK-3/CRMP2 pathway. Statistical significance: $^*P < 0.05$; $^{**}P < 0.01$; $^{***}P < 0.001$.

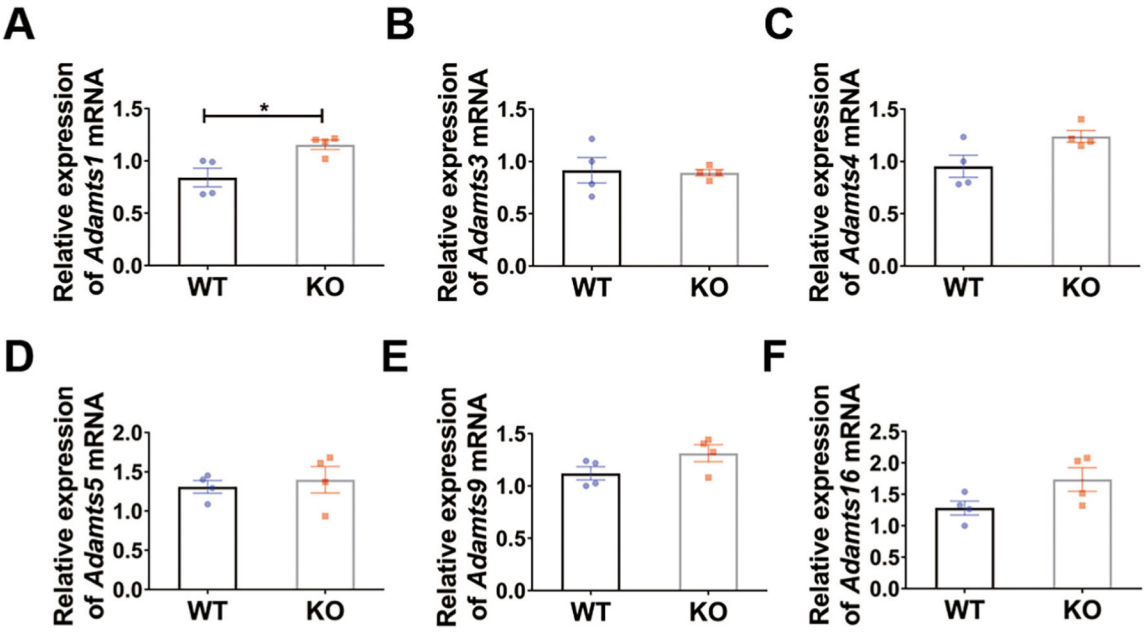

Fig. 6.

Relative expression of *Adamts* genes in *Adamts18* KO mice examined by qRT-PCR. Relative expression levels of *Adamts1* mRNA (A), *Adamts3*mRNA (B), *Adamts4* mRNA (C), *Adamts5* mRNA (D), *Adamts9* mRNA (E), and *Adamts16* mRNA (F) in embryonic brains of WT and *Adamts18* KO mice (n = 4/group) measured by quantitative RT–PCR. Relative expression level of each target gene was normalized to the expression level of the housekeeping gene *Gapdh* using the $\Delta\Delta C_t$ method. Data are presented as mean ± SEM. *P < 0.05.

Table 1.

Primary antibodies used in this study

No.	Product name	Application	Species	Dilution	Source
1	Anti-laminin	IHC	Rabbit	1:1000	Abcam Ab11575
		WB	Rabbit	1:1000	Abways AB0037
2	Anti-AKT	WB	Rabbit	1:1000	CST #9272
3	Anti-GSK3β	WB	Rabbit	1:1000	CST #9315
4	Anti-CRMP2	WB	Rabbit	1:1000	Abcam Ab62661
5	Anti-MAP2	IHC	Rabbit	1:1000	Abcam Ab32454
6	Anti-Tau	IHC	Rabbit	1:800	Abcam Ab32057
7	Phospho-specific anti-PI3K(Tyr458)	WB	Rabbit	1:1000	CST #4228
8	Anti-AKT(Ser473)	WB	Rabbit	1:1000	CST #9271
9	Anti-GSK3β(Ser9)	WB	Rabbit	1:1000	CST #9336
10	Anti-CRMP2(Thr514)	WB	Rabbit	1:1000	CST #9397
11	Anti-PSD95	WB	Rabbit	1:500	CST #3409
12	Anti-GAPDH	WB	Rabbit	1:5000	Abways AB0037

Table 2.

Primers for quantitative real-time RT-PCR

Genes	Primers	Product length (bp)
Lama1	Forward: 5′ GCTATCCTGCCCACATCAAAC 3′ Reverse: 5′ CAAGGACTGCACTTGTGAGC 3′	104
Lama3	Forward: 5′ CTCCAATGACCTCAGTCCAGAA 3′ Reverse: 5′ TCTCAGAACGATGCGGAACA 3′	86
Lama5	Forward: 5′ TTGGAGAATGGCGAGATTGTG 3′ Reverse: 5′ CGAAGTAACGGTGAGTAGGAGA 3′	80
Lamb1	Forward: 5′ TCTGTGAACCATGTACCTGTGA 3′ Reverse: 5′ GACACTGACCAGCAATGAGAC 3′	99
Lamc1	Forward: 5′ TGCCGCCAATGTGTCAATC 3′ Reverse: 5′ TGCCACTCGTACAATGTCATC 3′	130
Adamts1	Forward: 5′ GGGAAAGCCATCAGGACCAGGA 3′ Reverse: 5′ TTAGACCGCTGCCGTGGAAGT 3′	119
Adamts3	Forward: 5′ TCTACCACAGGGAGTCGGACCT 3′ Reverse: 5′ CGCCGCATTGTCTTGTTCAGC 3′	91
Adamts4	Forward: 5′ TCGCTTCCGCTCCTGCAACA 3′ Reverse: 5′ TGAAGAGGTCGGTTCGGTGGTT 3′	101
Adamts5	Forward: 5′ GCATCCAAGCCCTGGTCCAAAT 3′ Reverse: 5′ GGTGGCATCGTAGGTCTGTCCT 3′	141
Adamts9	Forward: 5′ TGCCAAGCCTCACCATGTCCT 3′ Reverse: 5′ TCCTCTGCTACGCATACCACCT 3′	113
Adamts16	Forward: 5′ GCAACCCCAAGACACGACCT 3′ Reverse: 5′ ACACGCTCCAGTTTCCCACA 3′	90
Gapdh	Forward: 5′ GTGGAGTCATACTGGAACATGTAG 3′ Reverse: 5′ AATGGTGAAGGTCGGTGTG 3′	150

Table 3.

Behavior tests of *Adamts18* KO mice

Behavioral tests	Function	Measurements	KO mice
Open field test	Anxiety	Total distance	+
		Average velocity	+
		Central distance %	+
		Central time %	+
		Central entries	+
Elevated O maze	Anxiety	Time spent in open arms	N.S.
Light/dark transition test	Anxiety	Time spent in light box	N.S.
Tail suspension test	Depression	Immobility time	−
Forced swim test	Depression	Immobility time	−
Sucrose preference test	Depression	Sucrose preference	+
Three-chamber test	Sociability and social novelty	Time spent in chamber	N.S.
Novel object recognition test	Recognition memory	Exploratory preference %	N.S.
Radial eight-arm maze test	Working memory	Testing Error%	N.S.
		Testing time	N.S.
Morris water maze test	Spatial memory	Latency to find platform	+
		Quadrant time %	N.S.
		Platform crossings	N.S.